Towards Robust Sensor-Fusion Ground SLAM: A Comprehensive Benchmark and A Resilient Framework

Deteng Zhang[1†], Junjie Zhang[2†], Yan Sun[3], Tao Li[4], Hao Yin[5], Hongzhao Xie[5] and Jie Yin[5*]

Abstract— Considerable advancements have been achieved in SLAM methods tailored for structured environments, yet their robustness under challenging corner cases remains a critical limitation. Although multi-sensor fusion approaches integrating diverse sensors have shown promising performance improvements, the research community faces two key barriers: On one hand, the lack of standardized and configurable benchmarks that systematically evaluate SLAM algorithms under diverse degradation scenarios hinders comprehensive performance assessment. While on the other hand, existing SLAM frameworks primarily focus on fusing a limited set of sensor types, without effectively addressing adaptive sensor selection strategies for varying environmental conditions.

To bridge these gaps, we make three key contributions: First, we introduce M3DGR dataset: a sensor-rich benchmark with systematically induced degradation patterns including visual challenge, LiDAR degeneracy, wheel slippage and GNSS denial. Second, we conduct a comprehensive evaluation of forty SLAM systems on M3DGR, providing critical insights into their robustness and limitations under challenging real-world conditions. Third, we develop a resilient modular multi-sensor fusion framework named Ground-Fusion++, which demonstrates robust performance by coupling GNSS, RGB-D, LiDAR, IMU (Inertial Measurement Unit) and wheel odometry. All codes [1] and datasets [2] are publicly available.

I. INTRODUCTION

Ground robots demonstrate significant potential in executing complex tasks such as industrial inspection, catering services, and agricultural automation [1]–[3], where robust localization is the most fundamental requirement. Recent advances in multi-sensor fusion SLAM (Simultaneous Localization and Mapping) [4]–[6] have shown promising results in controlled environments. However, as revealed in [7], [8], these systems exhibit critical vulnerabilities when confronting real-world challenges like temporary sensor failures or environmental extremes.

Existing benchmarking efforts face dual limitations: From the dataset perspective, predominant datasets [9], [10] emphasize common operational scenarios with fixed sensor configurations, lacking configurable rich sensor suites for algorithm customization and degradation scenarios for failure analysis. On the algorithmic front, although multi-sensor fusion strategies (loosely/tightly-coupled) which leverage complementary characteristics of heterogeneous sensors are demonstrated to be effective in enhancing localization performance, the question of optimal sensor selection [8], [10]

* Corresponding author: **Jie Yin** (`robot_yinjie@outlook.com`)
† Equal contribution. [1]Independent, [2]Chongqing University, [3]Nankai University, [4]Zhejiang University of Technology, [5]Shanghai Jiao Tong University
[1]https://github.com/sjtuyinjie/Ground-Fusion2
[2]https://github.com/sjtuyinjie/M3DGR

under specific degradation scenarios remains relatively understudied.

To fill these gaps, we introduce a novel challenging SLAM dataset **M3DGR**: a **M**ulti-sensor, **M**ulti-scenario and **M**assive-baseline SLAM dataset for **G**round **R**obot with a full sensor suite, incorporating systematically designed corner cases that induce sensor degradation scenarios. Furthermore, we conduct extensive evaluations of cutting-edge SLAM algorithms across diverse sensor configurations based on our dataset, providing critical insights into their respective limitations. Moreover, we develop a modular multi-sensor fusion SLAM framework named **Ground-Fusion++** to facilitate future research in SLAM. We summarize the core contributions of this work as follows:

- We launch a comprehensive SLAM benchmark named M3DGR for ground robots, featuring a rich sensor suite that includes an RGBD-IMU sensor, an omnidirectional camera, two non-repetitive scanning LiDARs, a wheel odometer, and two GNSS receivers. Furthermore, M3DGR covers challenging sensor-degeneration scenarios, such as visual degradation, LiDAR-degeneracy, wheel slippage and GNSS-denial.

- We conduct systematic evaluation with **forty** cutting-edge SLAM algorithms with diverse sensor configurations on our dataset. A thorough analysis is performed to evaluate these algorithms, as to provide key insights to their robustness and limitations under diverse challenging scenarios.

- We develop a resilient modular SLAM framework named Ground-Fusion++, which integrates GNSS, RGB-D camera, IMU, wheel odometer and LiDAR. This system achieves robust localization and promising mapping in large-scale environments, establishing a strong and adaptable baseline for future research in multi-sensor fusion SLAM.

II. RELATED WORK

A. SLAM Benchmark Datasets

High-quality benchmark datasets serve as critical catalysts for advancing SLAM research by enabling comprehensive comparisons. Although numerous multi-sensor SLAM datasets exist, they suffer from limitations including obsolescence, insufficient data volume, and inadequate coverage of challenging scenarios. For instance, early datasets such as EuRoC [11], and TUM-VI [11] cover limited sensor types and only support evaluation of vision-based methods. The OpenLORIS-Scene [13] and Ground-Challenge [10] datasets

TABLE I: Comparison with other SLAM benchmark datasets.

Dataset/Year	Scenario				Sensors							Number of compared algorithms
	VC[1]	LR[2]	GD[3]	WS[4]	RGB	Depth	Omni[5]	IMU	LiDAR	Wheel	GNSS	
EuRoC [11], 2016	✓				✓			✓				0
UrbanLoco [12], 2020	✓		✓		✓			✓	1		✓	3
OpenLoris-Scene [13], 2020	✓			✓	✓	✓		✓		✓		9
M2DGR [14], 2021	✓	✓	✓		✓		✓	✓	1		✓	*10*
FusionPortable [15], 2022	✓				✓			✓	1		✓	5
Ground-Challenge [10], 2023	✓	✓		✓	✓	✓		✓				5
M2DGR-Plus [8], 2024	✓		✓	✓	✓	✓		✓	1	✓	✓	6
MARS-LVIG [16], 2024	✓	✓			✓			✓	1		✓	6
M3DGR(Ours), 2025	✓	✓	✓	✓	✓	✓	✓	✓	2	✓	✓	**40**

[1] is visual challenge, [2] is LiDAR degeneracy, [3] is GNSS denied zone, [4] is wheel slippage and [5] is omnidirectional camera.

further extend sensor types, but their (pseudo-)ground-truth trajectories are calculated from LiDAR-based SLAM, which can sometimes be inaccurate. These limitations have restricted existing benchmarks to narrow evaluations of limited algorithm categories. More recently, datasets such as M2DGR [14] and MARS-LVIG [16] have gained attention for their richer sensor suites and more diverse environments, broadening support for more SLAM categories. However, they lack systematic evaluation for extreme conditions, limiting their effectiveness in assessing robustness in real-world degradation scenarios. As summarized in Table I, most existing benchmark do not provide sufficient algorithm coverage, leaving gaps in evaluating the adaptability of multi-sensor SLAM systems under adverse conditions.

With the rapid progress in multi-sensor fusion SLAM [5], [8], [17]–[19], there is a growing demand for a standardized benchmark with comprehensive evaluations across diverse sensor configurations. Although large-scale evaluations for SLAM are inherently tedious, time-consuming and resource-intensive, they are essential for ensuring rigorous performance assessment and driving future advancements in the field.

To address above needs, this work introduces M3DGR, a sensor-rich dataset designed specifically to evaluate the robustness of SLAM under systematically induced sensor degradation scenarios. As shown in Table II, M3DGR exhibits a higher level of degradation compared to existing datasets, providing a more challenging testbed for SLAM algorithms. Additionally, we conduct a large-scale evaluation of **forty** advanced SLAM algorithms. To ensure reproducibility, we will release all our custom algorithm implementations for M3DGR upon paper acceptance.

Degeneration Metric	M3DGR (Ours)	Baseline[1]
Visual (avg. keypoints/frame) ↓	**117**	138
LiDAR (avg. LiDAR matching error) ↑	**0.14**	0.04
Wheel (drift rate, m) ↑	**10.24**	2.04
GNSS (avg. valid satellites num.) ↓	**4**	13

TABLE II: Comparison of degradation levels between M3DGR and baseline datasets across different sensor modalities.

[1] Visual and wheel odometry baseline sequences are from [10], GNSS baseline sequences from [8], and LiDAR baseline is from [14]. Arrows indicate higher degradation levels.

B. Multi-sensor Fusion SLAM Algorithm

Over the past decade, visual SLAM [27], [28] and visual-inertial odometry (VIO) [29], [30] have achieved centimeter-level localization accuracy in small-scale indoor environments [9], [11], while LiDAR-based SLAM and LiDAR-Inertial-Odometry (LIO) [31]–[33] have demonstrated greater stability in large-scale outdoor scenarios. Recent advances have focused on multi-sensor fusion, particularly LiDAR-visual fusion [4], [34], [35], to enhance localization accuracy and mapping quality. Beyond LiDAR-vision fusion, integrating wheel odometry [24], [36] into VIO system further improves robustness in featureless or low-light environments, and GNSS integration [18], [19], [37], [38] enables global drift-free pose estimation. We provide curated overviews of leading LiDAR-visual SLAM and wheel-integrated SLAM at [3] and [4], respectively, which we do not elaborate on here. Recent studies have revealed that these cutting-edge SLAM systems struggle with significant drift or even complete tracking failures under specific sensor degradation scenarios [8], [10]. In GNSS-denied areas, LiDAR degeneracy, or severe motion blur, conventional SLAM approaches often fail to initialize or lose tracking, severely limiting their reliability in real-world applications.

To mitigate these challenges, recent works [5], [8], [26] have explored degeneration detection strategies aimed at improving system robustness. For example, Ground-Fusion [8] tightly integrates RGB-D, IMU, wheel odometry and GNSS, and employs an adaptive sensor selection strategy to enhance performance in corner cases. However, Ground-Fusion still faces challenges in ensuring long-term localization and mapping stability in large-scale outdoor environments, which is critical for downstream applications such as navigation and exploration [39].

Building on these insights, we introduce Ground-Fusion++, a degradation-aware multi-sensor fusion SLAM framework that extends Ground-Fusion by incorporating LiDAR alongside RGB-D, IMU, wheel odometry, and GNSS. By leveraging an adaptive sensor selection strategy, Ground-Fusion++ enables resilient localization on long-term outdoor trajectories. Furthermore, Ground-Fusion++ achieves real-time dense colorized mapping by seamlessly incorporating advanced rendering techniques [40], effectively addressing the limitations of its predecessor. A detailed comparative analysis of these systems is provided in Table III.

[3] https://github.com/sjtuyinjie/awesome-LiDAR-Visual-SLAM
[4] https://github.com/sjtuyinjie/awesome-Wheel-SLAM

TABLE III: Comparison with other multi-sensor fusion SLAM systems.

Method/Year	RGB	IMU	Depth	Wheel	GNSS	LiDAR	Open-source	Degradation-aware	Mapping
VINS-RGBD [20], 2019	✓	✓	✓				✓		SPC[1]/Non-color
DRE-SLAM [21], 2019	✓		✓	✓			✓		Mesh/Non-color
GR-Fusion [22], 2021	✓	✓		✓	✓	✓			SPC/Non-color
LVI-SAM [23], 2021	✓	✓				✓	✓		SPC/Non-color
VIW-Fusion [24], 2022	✓	✓		✓			✓		SPC/Non-color
R3LIVE [25], 2022	✓	✓				✓	✓		**Mesh/Color**
DAMS-LIO [26], 2023		✓		✓		✓		✓	SPC/Non-color
M2C-GVIO [19], 2023	✓	✓			✓				Sparse/Non-color
Ground-Fusion [8], 2024	✓	✓	✓	✓	✓		✓	✓	*DPC[2]*/Color
LIGO [18], 2025		✓			✓	✓	✓		SPC/Non-color
Ground-Fusion++(Ours), 2025	✓	✓	✓	✓	✓	✓	✓	✓	**Mesh/Color**

[1] SPC stands for Sparse Point Cloud, [2] DPC stands for Dense Point Cloud.

III. M3DGR BENCHMARK DATASET CONSTRUCTION

A. Acquisition Platform

As shown in Figure 1, we have constructed a ground robot equipped with multiple sensors to capture comprehensive datasets, including RGBD images, 3D point clouds, wheel odometry, and raw GNSS signals. Data acquisition and recording are managed by a high-performance Intel NUC with a high-speed NMVe SSD.

B. Sensor Setup

The physical design and sensor layouts of the ground robot are illustrated in Figure 1. The platform is equipped with a differential drive system, featuring two motorized wheels that provide wheel odometry data. For visual data collection, an RGBD-IMU sensor captures forward-facing images along with inertial measurements. Furthermore, two non-repetitive scanning Livox LiDARs are mounted to generate high-resolution 3D point clouds of the surrounding environment. To obtain raw GNSS signals, a GNSS receiver is equipped on the top of the robot. To ensure accurate ground-truth trajectories, high-precision trajectory data is obtained using a motion capture (Mocap) system for indoor experiments and a Real-Time Kinematic (RTK) receiver in outdoor environments as shown in Figure 2(b). A detailed overview of the specifications of all sensors and tracking devices is provided in Table IV.

TABLE IV: Sensor and Tracking Device Specifications

Device	Type	Spec.	Freq.(Hz)
RGBD-IMU sensor	Realsense D435i	RGB: 640*480, 69°(H) × 42°(H)	30
		Depth: 640*480, 87°(H) × 58°(V)	30
		IMU: 6-axis	200
Omnidirectional Camera	Insta360 X4	RGB: 2880x1440, 360°	15
LiDAR	Livox Avia	Non-repetitive, 450m, 70.4°(H) × 77.2°(V)	15
		IMU(BMI088): 6-axis	200
	Livox MID360	Non-repetitive, 40m, 360°(H) × 59°(V)	15
		IMU(ICM40609): 6-axis	200
Wheel Odometer	WHEELTEC	2D	20
GNSS Receiver	CUAV C-RTK 9Ps	BDS/GPS/GLONASS/Galileo	10
RTK Receiver	CUAV C-RTK 2HP	localization accuracy 0.8cm(H)/1.5cm(V)	15
Mocap System	Optitrack	localization accuracy 1mm	360

C. Synchronization

We use the rosbag tool in the Robot Operating System (ROS) to record data from all sensors, ensuring a unified timestamp mechanism for synchronization. Some sensors feature built-in hardware synchronization capabilities. For example, the RealSense D435i, which integrates an RGBD camera and a 6-axis IMU, achieves internal synchronization by simultaneously triggering data acquisition. Similarly, the two Livox LiDARs, each equipped with a 6-axis IMU, employ hardware triggering to capture data at the same instance, ensuring internal synchronization.

D. Data collection

We deploy our ground robot in both standard and challenging environments to collect a diverse dataset. An overview of the recorded sequences is presented in Table V. The corner cases in our dataset are classified into four categories: visual challenges, LiDAR degeneracy, wheel slippage, and GNSS-denied conditions, covering both indoor and outdoor scenarios. In addition to these challenging cases designed to test system robustness, our dataset also includes representative standard scenarios for evaluation. To provide an overview of outdoor sequences, Figure 2(a) illustrates the recorded trajectories on a map.

Visual challenge The dataset includes four types of visual challenges: low-light conditions, varying illumination, dynamic scenes, and occlusion. These scenarios are designed to test the resilience of vision-based perception systems in both indoor and outdoor environments. For indoor sequences, low-light conditions are simulated by turning off the room lights and using only a mobile phone flashlight for illumination. Varying illumination is introduced by alternating the room lights at regular intervals. To create dynamic scenes, a person moves continuously in front of the ground robot, disrupting its field of view. Additionally, occlusion scenarios are generated by deliberately blocking the camera. For outdoor sequences, low-light and varying illumination challenges are captured during nighttime operations. Low-light scenarios are recorded in dark environments, as shown in Figure 3(b), while varying illumination sequences are obtained by navigating the robot through areas with different lighting conditions. Dynamic environments are simulated by recording sequences with multiple pedestrians, cyclists, and moving vehicles, as illustrated in Figure 3(c). To induce occlusion, the camera is partially obstructed at various points during data collection.

LiDAR degeneracy The dataset includes two LiDAR degeneracy scenarios: a long corridor and an elevator transition. In the first scenario, the ground robot navigates through a long corridor, where the lack of geometric features poses
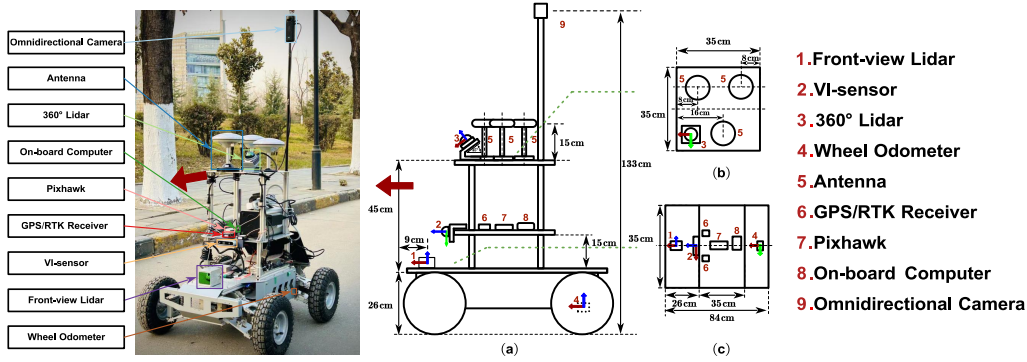
Fig. 1: Physical drawings and schematics of the ground robot. (a) Side view of the robot. (b) Sensor arrangement on the top layer. (c) Sensor arrangement on the middle and bottom layers. All dimensions are provided in centimeters.

TABLE V: An overview of scenarios in M3DGR dataset.

Scenario	Visual Challenge				LiDAR Degeneracy		Wheel Slippage				GNSS Denial	Standard	TOTAL
	Dark	VI[1]	Dynamic	Occlusion	Corridor	Elevator	WF[2]	ST[3]	Grass	RR[4]			
Number	5	4	3	4	2	1	2	2	2	1	2	4	32
Dist/m	1653.31	1055.58	355.97	1091.24	545.64	470.64	101.55	170.88	318.91	457.35	1162.39	4485.49	11868.95
Duration/s	2274	1458	609	1224	696	699	171	238	459	533	1359	5101	14821
Size/GB	27.0	20.0	7.1	12.3	11.9	11.2	3.3	2.9	9.7	10.4	23.2	86.0	225.0
GroundTruth	RTK/Mocap	RTK/Mocap	RTK/Mocap	RTK/Mocap	ArUco	ArUco	Mocap	Mocap	RTK	RTK	ArUco	RTK	—–

[1] stands for varying illumination, [2] stands for wheel float, [3] stands for sharp turn, [4] stands for rough road.
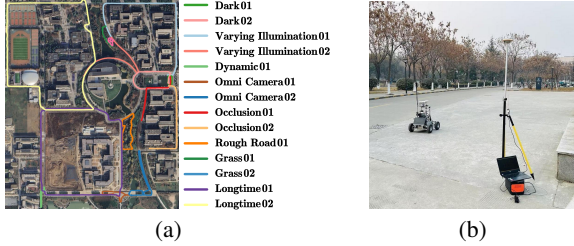

(a)　　　　　　　　　(b)

Fig. 2: (a) We visualize the trajectories of outdoor sequences in the map with different colors. (b) The ground truth for outdoor sequences was obtained using a geodetic-grade GNSS receiver in RTK mode, ensuring centimeter-level positioning accuracy.

(a)　　　(b)　　　(c)　　　(d)

(e)　　　(f)　　　(g)　　　(h)

Fig. 3: Diverse scenarios included in our datasets: (a) Normal lighting conditions. (b) Low-light environment. (c) A park with significant pedestrian dynamics. (d) An area without GNSS signal coverage. (e) An elevator. (f) A narrow corridor. (g) A grassy terrain. (h) A road with abrupt elevation changes.

challenges for LiDAR-based localization, as illustrated in Figure 3(f). The second scenario involves the robot moving from a long corridor into an elevator, introducing a sudden shift from a structured environment to a feature-sparse vertical space, as shown in Figure 3(e). To assess SLAM algorithm performance under these conditions, the robot is operated along a loop, returning to its starting

position. The relative transformation between the initial and final frames, computed using ArUco marker detection, serves as the quantitative metric for evaluating trajectory accuracy.

Wheel slippage The dataset captures four distinct wheel slippage scenarios: wheel float, sharp turns, grass-covered surfaces, and rough roads. Wheel float is induced by lifting the robot's driving wheels, causing intentional wheel slippage. Sharp turns are executed by commanding the robot to make rapid directional changes at high speeds, highlighting dynamic slippage behavior. Grass-covered surfaces introduce varying traction conditions as the robot navigates through uneven terrain, as shown in Figure 3(g). Rough roads, characterized by significant elevation changes, further challenge the robot's mobility, as illustrated in Figure 3(h).

GNSS denial The dataset includes a GNSS-denied scenario in which the ground robot begins in a GNSS-available area, traverses a GNSS-denied region (illustrated in Figure 3(d)), and then returns to its starting point. To evaluate localization performance, the relative transformation between the start and end positions is measured using ArUco marker detection, as previously described

IV. GROUND-FUSION++ SYSTEM DESIGN

To provide a resilient baseline system for the M3DGR benchmark, we develop Ground-Fusion++, a modular and degradation-aware multi-sensor fusion framework. Inspired by [23], [26], Ground-Fusion++ avoids a fully tightly coupled multi-sensor fusion approach and instead employs a hybrid framework consisting of an enhanced VIO subsystem and a LIO subsystem. We adopt Ground-Fusion [8] as the powerful visual odometry module and utilize a continuous-time version of Fast-LIO2 [31], which leverages advancements from [41], as the LIO subsystem.

Our system follows a LiDAR-priority selection strategy, where LIO is the primary source of pose estimation unless

LiDAR degradation is detected. If LiDAR degeneration occurs, the system adaptively switches to the enhanced VIO subsystem (Ground-Fusion), provided it can be successfully initialized. The VIO subsystem retains degradation detection and adaptive sensor selection strategies from Ground-Fusion [8], leveraging RGBD, GNSS, IMU and wheel odometry to ensure robustness.

To determine whether LiDAR degradation occurs, we evaluate the following condition:

$$\text{Deg}(t) = \begin{cases} 1, & \text{if } N_t^{\text{feat}} < \tau_N \text{ OR } \varepsilon_t^{\text{align}} > \tau_\varepsilon \\ 0, & \text{otherwise} \end{cases} \quad (1)$$

where N_t^{feat} denotes the LiDAR feature count at time t, $\varepsilon_t^{\text{align}} = \frac{1}{N} \sum_{i=1}^{N} \|p_i - q_i\|^2$ represents the ICP alignment residual with p_i and q_i being corresponding point pairs between consecutive scans, N is the total number of matched points, and τ_N, τ_ε are empirical thresholds for feature count and alignment error respectively.

To ensure consistent frame alignment between subsystems, we formulate the coordinate transformation optimization as follows:

$$T_{\text{align}} = \underset{T \in SE(3)}{\arg\min} \sum_{k=1}^{K} \rho \left(\left\| \log \left(T_{\text{LIO}}^k (T_{\text{VIO}}^k)^{-1} \right) \right\|_{\Sigma_k^{-1}}^2 \right) \quad (2)$$

where $T_{\text{align}} \in SE(3)$ represents the optimal coordinate transformation from LIO frame to VIO frame, $T_{\text{LIO}}^k, T_{\text{VIO}}^k \in SE(3)$ denote pose estimates from LIO and VIO subsystems at time k, $\Sigma_k \in \mathbb{R}^{6 \times 6}$ is the uncertainty covariance matrix. $\rho(\cdot)$ denotes the Cauchy robust kernel. $\|v\|_{\Sigma^{-1}}$ is the Mahalanobis norm.

For smooth trajectory transitions, we use an exponential map-based correction:

$$T_t^{\text{fused}} = T_t^{\text{active}} \exp \left(-\beta \left[\log \left((T_t^{\text{active}})^{-1} T_{\text{align}} T_t^{\text{backup}} \right) \right]^\wedge \right) \quad (3)$$

where $T_t^{\text{active}}/T_t^{\text{backup}} \in SE(3)$ are poses from active/backup subsystems. $\beta \in [0,1]$ is the smoothing factor.

Finally, the RGB images, LiDAR point clouds, and odometry outputs from the active subsystem are fed into the rendering module [40] to generate real-time, dense, colorized maps. Although Ground-Fusion++ primarily builds upon existing frameworks, **its modular design and comprehensive sensor integration ensure strong scalability and flexibility**. In particular, the carefully designed degradation detection mechanism and trajectory smoothing strategy effectively mitigate the impact of sensor failures and subsystem switching, ensuring robust and seamless localization performance. This architecture allows the LIO subsystem, VIO subsystem, and rendering module to be seamlessly upgraded with the latest advancements, establishing an adaptable baseline for future developments.

V. EXPERIMENTS AND EVALUATIONS

To systematically validate the effectiveness of the proposed M3DGR benchmark, we evaluate cutting-edge SLAM systems on ten sequences selected from M3DGR dataset. The characteristics of these sequences are summarized in Table VI. Quantitative results comparing all baselines are presented in Table VII.

A. Baselines

we conducted comprehensive evaluations across three SLAM categories: vision-based approaches, LiDAR-based approaches, and LiDAR-vision fusion systems. For vision-based methods, we assess pure visual odometry [42] and visual-inertial odometry systems [28]–[30], [43], along with their extensions incorporating [20], GNSS [37], or wheel odometry [24], [44]. In particular, Ground-Fusion [8] is a tightly-coupled RGB-Depth-Wheel-IMU-GNSS system within a factor graph. For LiDAR-based methods, we evaluate classical LiDAR SLAM [45]–[47] and LIO approaches [31], [41], [48]–[60]. For LiDAR-visual SLAM, both tightly-coupled frameworks [4], [34], [35], [61], [62] and loosely-coupled [23] are evaluated, along with our proposed system. Furthermore, Additionally, we evaluate wheel odometry integration and GNSS-based Single Point Positioning (SPP) solutions.

B. Benchmark Tests

Overall Performance: Most vision-based methods [29], [30], [42] perform well in small-scale environments with abundant visual features but struggle in challenging scenarios, often leading to tracking failures. In contrast, Ground-Fusion [8] achieves more stable localization, benefiting from multi-sensor fusion, though it still drifts sometimes. LiDAR-based SLAM generally offers higher localization accuracy, particularly in large-scale outdoor environments. Among the evaluated methods, CT-LIO [41], HM-LIO [59] and IESKF-LIO [54] exhibit the most consistent and precise performance. Notably, continuous-time approaches [41], [47] yield smoother and more stable trajectories compared to discrete-time methods such as A-LOAM [45] and LIO-SAM [32]. For LiDAR-visual SLAM, R2LIVE [64], Ground-Fusion++, and Fast-LIVO2 [35] exhibit the most reliable performance. While their localization accuracy offers only marginal improvements over leading LiDAR-based methods like [41], [59], they significantly enhance mapping quality by leveraging RGB information, which enriched structural details.

Visual Challenge: As the scene transitions from the dynamic environment to the varying lighting conditions, darkness, and eventually complete occlusion, the availability of reliable feature points decreases progressively. Consequently, the average ATE RMSE of all tested vision-based SLAM algorithms steadily increases, as illustrated in Figure 4 (a). Notably, systems incorporating wheel odometry [8], [24], [44] demonstrate greater robustness in these visual challenges, demonstrating the effectiveness of multi-sensor fusion in improving SLAM performance.

LiDAR Degeneracy: In highly structured corridors(the *Corridor*01 sequence), LiDAR-based algorithms such as [31], [56] frequently experience severe drift or even complete localization failure due to the lack of distinctive geometric features for reliable pose estimation. Certain systems, including VoxelMap [55], HM-LIO [59], and Fast-LIVO2 [35], demonstrate better robustness in these cases. In the *Elevator*01 sequence, most systems fail when the elevator goes up. Only CT-LIO [41] maintains good localization,

TABLE VI: Sample sequences for evaluation.

Sequence	Dynamic01	Varying-illu01	Occlusion01	Dark01	Corridor01	Elevator01	Wheel-float01	Sha-turn01	Grass01	GNSS-denial01
Duration/s	175	154	142	206	403	699	123	138	287	609
Dist/m	72.22	73.69	65.00	112.94	332.32	470.64	45.01	98.31	189.45	524.37
Speed/s	0.41	0.47	0.45	0.55	0.82	0.67	0.36	0.71	0.66	0.86
Discription of features	indoor, dynamic pedestrians	indoor, varying light conditions	indoor, complete visual occlusion	outdoor, low light conditions	indoor, long corridor	indoor, long corridor with Elevator	indoor, tire slip	outdoor, quickly turn	outdoor, grass covered surface	outdoor, GNSS denied zones

TABLE VII: ATE RMSE(m) of SLAM systems on M3DGR sequences.

Method/Scenario	Visual Challenge				LiDAR Degeneration		Wheel Slippage			GNSS Denial
	Dynamic01	Varying-illu01	Dark01	Occlusion01	Corridor01	Elevator01	Wheel-float01	Sha-turn01	Grass01	GNSS-denial01
Wheel Odom	2.32	2.36	5.52	2.04	72.61	66.94	2.20	7.44	25.34	✗
GNSS SPP	✗	✗	7.69	✗	✗	✗	✗	✗	0.48	11.61
TartanVO [42], 2021	2.37	2.17	12.37	✗	✗	✗	1.93	2.09	4.68	✗
ORB-SLAM2 [43], 2017	0.14	✗	✗	✗	6.41	8.09	1.72	1.54	✗	✗
ORB-SLAM3 [28], 2021	✗	✗	✗	✗	✗	✗	✗	✗	✗	✗
DM-VIO [29], 2022	2.25	2.27	4.08	✗	12.20	2.54	✗	8.90	✗	✗
VINS-Mono [30], 2018	0.43	2.70	7.91	✗	9.82	62.80	0.46	0.36	2.17	30.36
VINS-RGBD [20], 2019	0.20	1.86	✗	✗	5.62	✗	0.28	0.35	7.52	26.31
GVINS [37], 2022	0.26	1.25	✗	✗	9.42	2.89	0.27	0.40	✗	✗
VIW-Fusion [24], 2022	0.62	1.02	0.77	✗	5.58	16.68	0.77	2.44	2.91	99.06
VINS-GPS-Wheel [44], 2021	1.18	1.32	15.55	✗	5.55	43.48	0.86	2.00	18.47	16.89
Ground-Fusion [8], 2024	0.19	0.59	1.10	1.21	26.25	29.93	0.29	1.16	1.33	13.19
A-LOAM [45], 2018	0.15	0.16	6.36	0.19	66.66	48.37	0.29	0.26	1.92	8.46
LOAM-Livox [46], 2020	2.88	3.24	2.55	2.42	43.91	87.52	1.47	1.78	4.36	✗
CTLO [47], 2023	0.10	0.12	0.15	0.14	3.29	52.31	0.18	0.15	1.34	0.88
LeGO-LOAM [48], 2018	7.92	✗	13.40	6.28	19.65	✗	5.89	8.40	32.66	95.91
LIO-mapping [49], 2019	2.03	1.95	✗	2.46	✗	✗	1.05	1.46	9.75	✗
LIO-SAM [32], 2020	5.10	2.24	✗	1.31	36.15	✗	0.73	0.63	1.34	43.21
LINS [50], 2020	10.18	3.40	13.25	5.07	✗	✗	5.03	5.04	87.04	✗
LiLi-OM [51], 2021	1.49	0.19	✗	7.00	✗	✗	0.35	2.08	2.22	15.96
LIO-Livox [52], 2021	0.18	0.72	0.30	0.47	✗	✗	0.35	11.25	1.32	6.63
Faster-LIO [53], 2022	0.12	0.13	0.17	0.11	✗	✗	2.19	2.84	1.33	5.60
IESKF-LIO [54], 2022	0.14	0.14	0.15	0.13	14.38	✗	0.17	0.16	1.32	0.08
VoxelMap [55], 2022	0.89	0.76	4.93	0.91	1.08	19.22	0.99	1.11	0.78	0.07
Fast-LIO2 [31], 2022	0.13	0.11	0.24	0.11	✗	✗	0.16	0.18	1.32	13.46
Point-LIO [56], 2023	0.14	0.14	0.29	0.15	9.58	✗	0.19	0.20	1.32	18.39
LOG-LIO [57], 2023	0.13	0.12	0.99	0.14	✗	✗	0.18	0.07	1.33	27.03
CT-LIO [41], 2023	0.12	0.12	0.18	0.13	3.56	2.39	0.13	0.10	1.34	2.71
DLIO [58], 2023	0.12	0.10	0.16	0.15	40.46	44.70	0.18	0.17	1.35	5.80
HM-LIO [59], 2023	0.12	0.15	0.17	0.14	3.23	✗	0.14	0.20	1.33	0.09
MM-LINS [60], 2024	2.84	2.79	0.27	1.95	✗	74.31	2.25	2.83	1.67	7.73
LIGO [18], 2025	0.10	0.12	0.25	0.16	9.55	43.34	0.19	0.17	1.33	11.75
LVI-SAM [23], 2021	0.85	136.03	4.23	30.85	7.06	28.44	0.64	0.49	7.63	12.56
R2LIVE [61], 2021	0.11	0.11	0.13	0.10	✗	✗	0.09	0.19	1.33	1.36
R3LIVE [25], 2022	8.76	4.24	1.12	9.00	6.07	✗	1.07	6.00	1.69	✗
Fast-LIVO [34], 2022	✗	8.95	✗	9.49	7.96	✗	0.78	1.92	1.50	✗
Coco-LIC [62], 2023	1.77	0.97	0.54	1.66	6.98	✗	0.64	1.80	1.21	0.54
SR-LIVO [63], 2024	1.23	0.28	0.09	1.31	✗	✗	0.86	✗	0.09	92.14
Fast-LIVO2 [35], 2024	0.44	0.28	0.17	0.33	3.35	✗	0.51	0.81	9.71	0.09
Ground-Fusion++(Ours),2025	0.09	0.09	0.17	0.10	6.19	5.28	0.10	0.09	1.33	5.20

with temporary vertical drift during elevator movement while keeping stable horizontal positioning.

Wheel Slippage: Most wheel odometry-integrated algorithms [24], [44] suffer from significant drift when encountering wheel slippage. However, Ground-Fusion [8] mitigates this issue through a wheel anomaly detection mechanism that filters out unreliable observations, as shown in Figure 4 (c). This highlights that even a simple degradation-handling method can significantly enhance robustness.

GNSS Denial: In GNSS-denied environments, most GNSS-integrated SLAM systems [37] experience substantial performance degradation due to the lack of absolute positioning updates. However, systems such as VINS-GPS-Wheel [44] and Ground-Fusion [8], which incorporate wheel odometry, exhibit reduced drift under these conditions by relying on additional motion constraints. Their trajectories on the GNSS-Denial01 sequence are presented in Figure 4(d).

TABLE VIII: Comparison of localization accuracy (m) under LiDAR degradation scenarios with different configurations.

Methods	corridor01†	corridor02†
LIO subsystem	6.14	26.66
Ground-Fusion++ with [65]	4.72	2.12
Ground-Fusion++ (Ours)	1.67	1.73

† Artificial noise was injected during two degradation intervals: 50–80s and 200–250s.

C. Effectiveness of Our System

Degeneration-adaptive Capability: To validate the robustness of our system under LiDAR degradation, we conduct comparative experiments using three configurations: the LIO subsystem alone, Ground-Fusion++ integrated with the degeneration detection method proposed in [65], and our full Ground-Fusion++ system with the proposed degeneration detection and adaptive sensor fusion strategy. As shown in Table VIII, our method achieves significantly better localization accuracy under harsh LiDAR degradation.
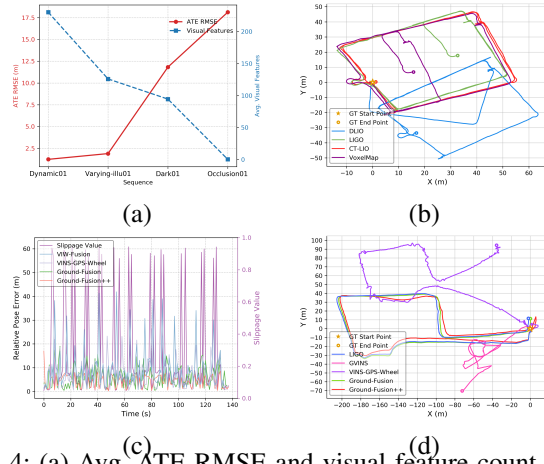
Fig. 4: (a) Avg. ATE RMSE and visual feature count across different challenging visual sequences. We set it as 20m if a system fails. (b) Trajectories of different LiDAR methods on the *Elevator*01 sequence. (c) Wheel slippage and RPE for different wheel-based methods. (d) Trajectories of different GNSS-integrated systems in the GNSS-denial01 sequence.

Long-term Capability: We conduct experiments on the *Longtime*01 sequence, which spans a trajectory of about 30 minutes in a large-scale outdoor campus environment. Our proposed system, Ground-Fusion++, achieves an ATE RMSE of 7.5m with adaptive sensor strategy, significantly outperforming Ground-Fusion (22.5m) [8]. Moreover, while Ground-Fusion fails to generate a dense map in this challenging scenario, Ground-Fusion++ successfully constructs a high-quality, colorized dense map, as shown in Figure 5(c).
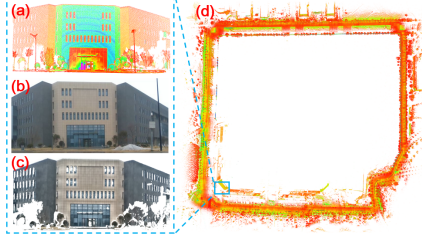

Fig. 5: The reconstruction results of Ground-Fusion++ on the *Longtime*01 sequence. (a) The input RGB image. (b) The corresponding point cloud. (c) The dense color mesh generated by Ground-Fusion++. (d) The full point cloud.

VI. CONCLUSION

This work presents M3DGR, a large-scale multi-sensor dataset for ground robot SLAM under challenging conditions. By systematically inducing sensor degradation scenarios, M3DGR enables in-depth evaluation of multi-sensor fusion algorithms. We evaluate 40 leading SLAM systems with diverse sensor settings across M3DGR, uncovering their limitations in extreme environments. To further support robust SLAM development, we propose Ground-Fusion++, a modular degradation-aware multi-sensor fusion framework with adaptive sensor selection, which demonstrates resilient localization and strong mapping ability.

REFERENCES

[1] C. Cadena, L. Carlone, H. Carrillo, Y. Latif, D. Scaramuzza, J. Neira, I. Reid, and J. J. Leonard, "Past, present, and future of simultaneous localization and mapping: Toward the robust-perception age," *IEEE Transactions on robotics*, vol. 32, no. 6, pp. 1309–1332, 2016.

[2] B. Al-Tawil, T. Hempel, A. Abdelrahman, and A. Al-Hamadi, "A review of visual slam for robotics: evolution, properties, and future applications," *Frontiers in Robotics and AI*, vol. 11, p. 1347985, 2024.

[3] J. Yin, C. Liang, X. Li, Q. Xu, H. Wang, T. Fan, Z. Wu, and Z. Zhang, "Design, sensing and control of service robotic system for intelligent navigation and operation in internet data centers," in *2023 IEEE 19th International Conference on Automation Science and Engineering (CASE)*. IEEE, 2023, pp. 1–8.

[4] J. Lin and F. Zhang, "R3live: A robust, real-time, rgb-colored, lidar-inertial-visual tightly-coupled state estimation and mapping package," *arXiv preprint arXiv:2109.07982*, 2021.

[5] J. Yin, T. Li, H. Yin, W. Yu, and D. Zou, "Sky-gvins: a sky-segmentation aided gnss-visual-inertial system for robust navigation in urban canyons," *Geo-spatial Information Science*, vol. 0, no. 0, pp. 1–11, 2023.

[6] D. Qu, C. Yan, D. Wang, J. Yin, Q. Chen, D. Xu, Y. Zhang, B. Zhao, and X. Li, "Implicit event-rgbd neural slam," in *Proceedings of the IEEE/CVF Conference on Computer Vision and Pattern Recognition*, 2024, pp. 19 584–19 594.

[7] N. Khedekar, M. Kulkarni, and K. Alexis, "Mimosa: A multi-modal slam framework for resilient autonomy against sensor degradation," in *2022 IEEE/RSJ International Conference on Intelligent Robots and Systems (IROS)*. IEEE, 2022, pp. 7153–7159.

[8] J. Yin, A. Li, W. Xi, W. Yu, and D. Zou, "Ground-fusion: A low-cost ground slam system robust to corner cases," in *2024 IEEE International Conference on Robotics and Automation (ICRA)*, 2024, pp. 8603–8609.

[9] D. Schubert, T. Goll, N. Demmel, V. Usenko, J. Stückler, and D. Cremers, "The tum vi benchmark for evaluating visual-inertial odometry," in *2018 IEEE/RSJ International Conference on Intelligent Robots and Systems (IROS)*. IEEE, 2018, pp. 1680–1687.

[10] J. Yin, H. Yin, C. Liang, H. Jiang, and Z. Zhang, "Ground-challenge: A multi-sensor slam dataset focusing on corner cases for ground robots," in *2023 IEEE International Conference on Robotics and Biomimetics (ROBIO)*. IEEE, 2023, pp. 1–5.

[11] M. Burri, J. Nikolic, P. Gohl, T. Schneider, J. Rehder, S. Omari, M. W. Achtelik, and R. Siegwart, "The euroc micro aerial vehicle datasets," *The International Journal of Robotics Research*, vol. 35, no. 10, pp. 1157–1163, 2016.

[12] W. Wen, Y. Zhou, G. Zhang, S. Fahandezh-Saadi, X. Bai, W. Zhan, M. Tomizuka, and L.-T. Hsu, "Urbanloco: A full sensor suite dataset for mapping and localization in urban scenes," in *2020 IEEE International Conference on Robotics and Automation (ICRA)*. IEEE, 2020, pp. 2310–2316.

[13] X. Shi, D. Li, P. Zhao, Q. Tian, Y. Tian, Q. Long, C. Zhu, J. Song, F. Qiao, L. Song, *et al.*, "Are we ready for service robots? the openloris-scene datasets for lifelong slam," in *2020 IEEE international conference on robotics and automation (ICRA)*. IEEE, 2020, pp. 3139–3145.

[14] J. Yin, A. Li, T. Li, W. Yu, and D. Zou, "M2dgr: A multi-sensor and multi-scenario slam dataset for ground robots," *IEEE Robotics and Automation Letters*, 2022.

[15] J. Jiao, H. Wei, T. Hu, X. Hu, Y. Zhu, Z. He, J. Wu, J. Yu, X. Xie, H. Huang, *et al.*, "Fusionportable: A multi-sensor campus-scene dataset for evaluation of localization and mapping accuracy on diverse platforms," in *2022 IEEE/RSJ International Conference on Intelligent Robots and Systems (IROS)*. IEEE, 2022, pp. 3851–3856.

[16] H. Li, Y. Zou, N. Chen, J. Lin, X. Liu, W. Xu, C. Zheng, R. Li, D. He, F. Kong, *et al.*, "Mars-lvig dataset: A multi-sensor aerial robots slam dataset for lidar-visual-inertial-gnss fusion," *The International Journal of Robotics Research*, p. 02783649241227968, 2024.

[17] X. Xu, L. Zhang, J. Yang, C. Cao, W. Wang, Y. Ran, Z. Tan, and M. Luo, "A review of multi-sensor fusion slam systems based on 3d lidar," *Remote Sensing*, vol. 14, no. 12, p. 2835, 2022.

[18] D. He, H. Li, and J. Yin, "Ligo: A tightly coupled lidar-inertial-gnss odometry based on a hierarchy fusion framework for global localization with real-time mapping," *IEEE Transactions on Robotics*, 2025.

[19] T. Hua, L. Pei, T. Li, J. Yin, G. Liu, and W. Yu, "M2c-gvio: motion manifold constraint aided gnss-visual-inertial odometry for ground vehicles," *Satellite Navigation*, vol. 4, no. 1, pp. 1–15, 2023.

[20] Z. Shan, R. Li, and S. Schwertfeger, "Rgbd-inertial trajectory estima-

tion and mapping for ground robots," *Sensors*, vol. 19, no. 10, p. 2251, 2019.

[21] D. Yang, S. Bi, W. Wang, C. Yuan, X. Qi, and Y. Cai, "Dre-slam: Dynamic rgb-d encoder slam for a differential-drive robot," *Remote Sensing*, vol. 11, no. 4, p. 380, 2019.

[22] T. Wang, Y. Su, S. Shao, C. Yao, and Z. Wang, "Gr-fusion: Multi-sensor fusion slam for ground robots with high robustness and low drift," in *2021 IEEE/RSJ International Conference on Intelligent Robots and Systems (IROS)*. IEEE, 2021, pp. 5440–5447.

[23] T. Shan, B. Englot, C. Ratti, and D. Rus, "Lvi-sam: Tightly-coupled lidar-visual-inertial odometry via smoothing and mapping," *arXiv preprint arXiv:2104.10831*, 2021.

[24] T. Zhuang, "Viw-fusion," https://github.com/TouchDeeper/VIW-Fusion, 2022.

[25] J. Lin and F. Zhang, "R 3 live: A robust, real-time, rgb-colored, lidar-inertial-visual tightly-coupled state estimation and mapping package," in *2022 International Conference on Robotics and Automation (ICRA)*. IEEE, 2022, pp. 10 672–10 678.

[26] F. Han, H. Zheng, W. Huang, R. Xiong, Y. Wang, and Y. Jiao, "Dams-lio: A degeneration-aware and modular sensor-fusion lidar-inertial odometry," in *2023 IEEE International Conference on Robotics and Automation (ICRA)*. IEEE, 2023, pp. 2745–2751.

[27] Z. Teed and J. Deng, "Droid-slam: Deep visual slam for monocular, stereo, and rgb-d cameras," *Advances in neural information processing systems*, vol. 34, pp. 16 558–16 569, 2021.

[28] C. Campos, R. Elvira, J. J. G. Rodríguez, J. M. Montiel, and J. D. Tardós, "Orb-slam3: An accurate open-source library for visual, visual–inertial, and multimap slam," *IEEE Transactions on Robotics*, 2021.

[29] L. Von Stumberg and D. Cremers, "Dm-vio: Delayed marginalization visual-inertial odometry," *IEEE Robotics and Automation Letters*, vol. 7, no. 2, pp. 1408–1415, 2022.

[30] T. Qin, P. Li, and S. Shen, "Vins-mono: A robust and versatile monocular visual-inertial state estimator," *IEEE Transactions on Robotics*, vol. 34, no. 4, pp. 1004–1020, 2018.

[31] W. Xu, Y. Cai, D. He, J. Lin, and F. Zhang, "Fast-lio2: Fast direct lidar-inertial odometry," *IEEE Transactions on Robotics*, vol. 38, no. 4, pp. 2053–2073, 2022.

[32] T. Shan, B. Englot, D. Meyers, W. Wang, C. Ratti, and D. Rus, "Lio-sam: Tightly-coupled lidar inertial odometry via smoothing and mapping," in *2020 IEEE/RSJ International Conference on Intelligent Robots and Systems (IROS)*. IEEE, 2020, pp. 5135–5142.

[33] P. Dellenbach, J.-E. Deschaud, B. Jacquet, and F. Goulette, "Ct-icp: Real-time elastic lidar odometry with loop closure," in *2022 International Conference on Robotics and Automation (ICRA)*. IEEE, 2022, pp. 5580–5586.

[34] C. Zheng, Q. Zhu, W. Xu, X. Liu, Q. Guo, and F. Zhang, "Fast-livo: Fast and tightly-coupled sparse-direct lidar-inertial-visual odometry," in *2022 IEEE/RSJ international conference on intelligent robots and systems (IROS)*. IEEE, 2022, pp. 4003–4009.

[35] C. Zheng, W. Xu, Z. Zou, T. Hua, C. Yuan, D. He, B. Zhou, Z. Liu, J. Lin, F. Zhu, *et al.*, "Fast-livo2: Fast, direct lidar-inertial-visual odometry," *IEEE Transactions on Robotics*, 2024.

[36] K. J. Wu, C. X. Guo, G. Georgiou, and S. I. Roumeliotis, "Vins on wheels," in *2017 IEEE International Conference on Robotics and Automation (ICRA)*. IEEE, 2017, pp. 5155–5162.

[37] S. Cao, X. Lu, and S. Shen, "Gvins: Tightly coupled gnss–visual–inertial fusion for smooth and consistent state estimation," *IEEE Transactions on Robotics*, 2022.

[38] H. Jiang, D. Yan, J. Wang, and J. Yin, "Innovation-based kalman filter fault detection and exclusion method against all-source faults for tightly coupled gnss/ins/vision integration," *GPS Solutions*, vol. 28, no. 3, pp. 1–17, 2024.

[39] J. Yin, A. Luo, Y. Du, A. Cherian, T. K. Marks, J. Le Roux, and C. Gan, "Disentangled acoustic fields for multimodal physical scene understanding," in *2024 IEEE/RSJ International Conference on Intelligent Robots and Systems (IROS)*. IEEE, 2024, pp. 557–564.

[40] J. Lin, C. Yuan, Y. Cai, H. Li, Y. Ren, Y. Zou, X. Hong, and F. Zhang, "Immesh: An immediate lidar localization and meshing framework," *IEEE Transactions on Robotics*, 2023.

[41] chengwei0427, "Ct-lio," https://github.com/chengwei0427/ct-lio.git, 2023.

[42] W. Wang, Y. Hu, and S. Scherer, "Tartanvo: A generalizable learning-based vo," in *Conference on Robot Learning*. PMLR, 2021, pp. 1761–1772.

[43] R. Mur-Artal and J. D. Tardós, "Orb-slam2: An open-source slam system for monocular, stereo, and rgb-d cameras," *IEEE transactions on robotics*, vol. 33, no. 5, pp. 1255–1262, 2017.

[44] Wallong, "Vins-gw," https://github.com/Wallong/VINS-GPS-Wheel, 2018.

[45] T. Qin and C. Shaozu, "A-loam," https://github.com/HKUST-Aerial-Robotics/A-LOAM, 2018.

[46] J. Lin and F. Zhang, "Loam livox: A fast, robust, high-precision lidar odometry and mapping package for lidars of small fov," in *2020 IEEE international conference on robotics and automation (ICRA)*. IEEE, 2020, pp. 3126–3131.

[47] chengwei0427, "Ctlo," https://github.com/chengwei0427/CTLO.git, 2023.

[48] T. Shan and B. Englot, "Lego-loam: Lightweight and ground-optimized lidar odometry and mapping on variable terrain," in *2018 IEEE/RSJ International Conference on Intelligent Robots and Systems (IROS)*. IEEE, 2018, pp. 4758–4765.

[49] H. Ye, Y. Chen, and M. Liu, "Tightly coupled 3d lidar inertial odometry and mapping," in *2019 International Conference on Robotics and Automation (ICRA)*. IEEE, 2019, pp. 3144–3150.

[50] C. Qin, H. Ye, C. E. Pranata, J. Han, S. Zhang, and M. Liu, "Lins: A lidar-inertial state estimator for robust and efficient navigation," in *2020 IEEE international conference on robotics and automation (ICRA)*. IEEE, 2020, pp. 8899–8906.

[51] K. Li, M. Li, and U. D. Hanebeck, "Towards high-performance solid-state-lidar-inertial odometry and mapping," *IEEE Robotics and Automation Letters*, vol. 6, no. 3, pp. 5167–5174, 2021.

[52] Livox, "Lio-livox," https://github.com/Livox-SDK/LIO-Livox, 2021.

[53] C. Bai, T. Xiao, Y. Chen, H. Wang, F. Zhang, and X. Gao, "Faster-lio: Lightweight tightly coupled lidar-inertial odometry using parallel sparse incremental voxels," *IEEE Robotics and Automation Letters*, vol. 7, no. 2, pp. 4861–4868, 2022.

[54] chengwei0427, "Ieskf-lio," https://github.com/chengwei0427/ESKF_LIO.git, 2022.

[55] C. Yuan, W. Xu, X. Liu, X. Hong, and F. Zhang, "Efficient and prob-abilistic adaptive voxel mapping for accurate online lidar odometry," *IEEE Robotics and Automation Letters*, vol. 7, no. 3, pp. 8518–8525, 2022.

[56] D. He, W. Xu, N. Chen, F. Kong, C. Yuan, and F. Zhang, "Point-lio: Robust high-bandwidth light detection and ranging inertial odometry," *Advanced Intelligent Systems*, vol. 5, no. 7, p. 2200459, 2023.

[57] K. Huang, J. Zhao, Z. Zhu, C. Ye, and T. Feng, "Log-lio: A lidar-inertial odometry with efficient local geometric information estimation," *IEEE Robotics and Automation Letters*, vol. 9, no. 1, pp. 459–466, 2023.

[58] K. Chen, R. Nemiroff, and B. T. Lopez, "Direct lidar-inertial odometry: Lightweight lio with continuous-time motion correction," in *2023 IEEE international conference on robotics and automation (ICRA)*. IEEE, 2023, pp. 3983–3989.

[59] chengwei0427, "Hm-lio," https://github.com/chengwei0427/hm-lio.git, 2023.

[60] Y. Ma, J. Xu, S. Yuan, T. Zhi, W. Yu, J. Zhou, and L. Xie, "Mm-lins: a multi-map lidar-inertial system for over-degenerate environments," *IEEE Transactions on Intelligent Vehicles*, 2024.

[61] J. Lin, C. Zheng, W. Xu, and F. Zhang, "R 2 live: A robust, real-time, lidar-inertial-visual tightly-coupled state estimator and mapping," *IEEE Robotics and Automation Letters*, vol. 6, no. 4, pp. 7469–7476, 2021.

[62] X. Lang, C. Chen, K. Tang, Y. Ma, J. Lv, Y. Liu, and X. Zuo, "Coco-lic: continuous-time tightly-coupled lidar-inertial-camera odometry using non-uniform b-spline," *IEEE Robotics and Automation Letters*, 2023.

[63] Z. Yuan, J. Deng, R. Ming, F. Lang, and X. Yang, "Sr-livo: Lidar-inertial-visual odometry and mapping with sweep reconstruction," *IEEE Robotics and Automation Letters*, 2024.

[64] J. Lin, C. Zheng, W. Xu, and F. Zhang, "R2live: A robust, real-time, lidar-inertial-visual tightly-coupled state estimator and mapping," *arXiv preprint arXiv:2102.12400*, 2021.

[65] S. Ji, W. Chen, Z. Su, Y. Guan, J. Li, H. Zhang, and H. Zhu, "A point-to-distribution degeneracy detection factor for lidar slam using local geometric models," in *2024 IEEE International Conference on Robotics and Automation (ICRA)*. IEEE, 2024, pp. 12 283–12 289.